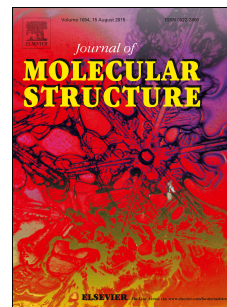


Journal Pre-proof

Synthesis, structure, computational and molecular docking studies of asymmetrically di-substituted ureas containing carboxyl and phosphoryl hydrogen bond acceptor functional groups

Obinna C. Okpareke, William Henderson, Joseph R. Lane, Sunday N. Okafor



PII: S0022-2860(19)31469-3

DOI: <https://doi.org/10.1016/j.molstruc.2019.127360>

Reference: MOLSTR 127360

To appear in: *Journal of Molecular Structure*

Received Date: 15 May 2019

Revised Date: 21 September 2019

Accepted Date: 2 November 2019

Please cite this article as: O.C. Okpareke, W. Henderson, J.R. Lane, S.N. Okafor, Synthesis, structure, computational and molecular docking studies of asymmetrically di-substituted ureas containing carboxyl and phosphoryl hydrogen bond acceptor functional groups, *Journal of Molecular Structure* (2019), doi: <https://doi.org/10.1016/j.molstruc.2019.127360>.

This is a PDF file of an article that has undergone enhancements after acceptance, such as the addition of a cover page and metadata, and formatting for readability, but it is not yet the definitive version of record. This version will undergo additional copyediting, typesetting and review before it is published in its final form, but we are providing this version to give early visibility of the article. Please note that, during the production process, errors may be discovered which could affect the content, and all legal disclaimers that apply to the journal pertain.

© 2019 Published by Elsevier B.V.

Synthesis, structure, computational and molecular docking studies of asymmetrically di-substituted ureas containing carboxyl and phosphoryl hydrogen bond acceptor functional groups

Obinna C. Okpareke^{1,2*}, William Henderson¹, Joseph R. Lane¹ and, Sunday N. Okafor³

¹*School of Science, University of Waikato, Private Bag 3105, Hamilton 3240, New Zealand*

²*Department of Pure and Industrial Chemistry, University of Nigeria, 410011 Nsukka, Enugu State, Nigeria*

³*Department of Pharmaceutical and Medicinal Chemistry, University of Nigeria, 410011 Nsukka, Enugu State, Nigeria*

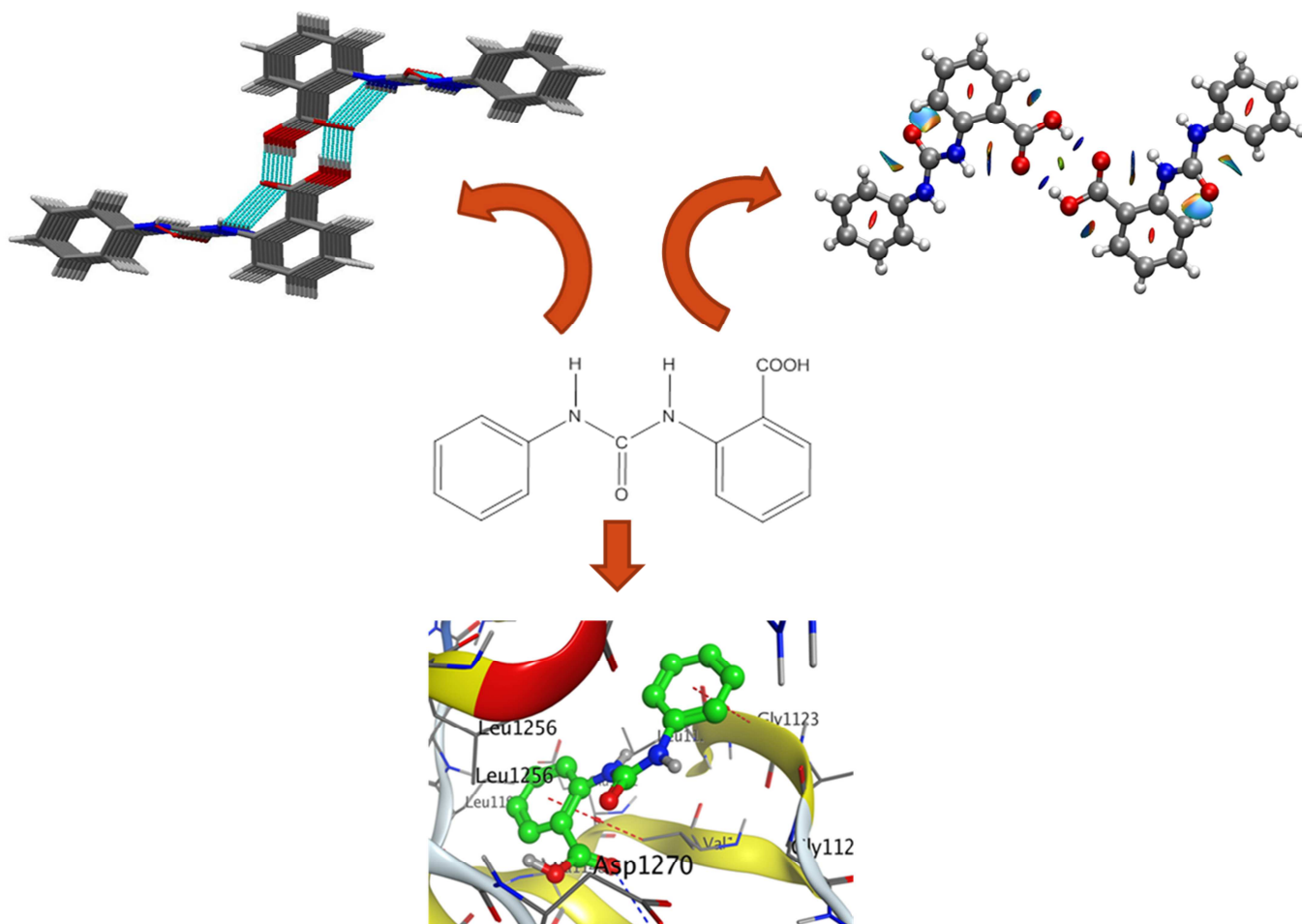
Corresponding author email: obinna.okpareke@unn.edu.ng

Abstract

Two asymmetrically substituted ureas *N,N'*-(2-carboxyl phenyl)phenyl urea (**L**₁) and diethyl 4-(3-phenylureido)benzylphosphonate (**L**₂) were synthesized and characterized by spectroscopic and X-ray crystallographic analysis. The two compounds crystallized in the centrosymmetric monoclinic crystal system and $P2_1/n$ space group. The carboxyl substituted urea **L**₁ crystallized with one molecule in the asymmetric unit. A hydrogen-bonded dimer is formed between the carboxyl group of the urea and a second molecule of the compound. The urea functional group is involved in both intramolecular and intermolecular hydrogen bonding with the carboxyl and carbonyl oxygens, respectively. The interplay of intermolecular and intramolecular hydrogen bonding in the compound results in a 2-D hydrogen-bonded structure. The phosphoryl-substituted urea **L**₂, on the other hand, crystallized with two molecules in the asymmetric unit, resulting in a hydrogen-bonded tetramer in the crystal lattice. Non-covalent interactions (NCI) analysis of the two compounds revealed the presence of competitive interactions between the urea functional group and the carboxyl and phosphoryl substituents in **L**₁ and **L**₂, respectively. Molecular docking calculations predicted favorable binding interactions between the ureas and the two anticancer protein targets EGFR kinase (2J5F) and anaplastic lymphoma kinase (5J7H).

Keywords: Synthesis, structure, non-covalent interaction, molecular docking

Graphical Abstract



1. Introduction

A wide range of biological and chemical interactions, including interactions between proteins and drugs, catalysts and their substrates, self-assembly of nanomaterials and even simple chemical reactions are dominated by non-covalent interactions. Among these interactions are hydrogen bonding, dipole-dipole interactions, steric repulsion, and London dispersions [1-3]. Hydrogen bonding, due to its molecular robustness, pronounced directionality and relatively high strength have been the subject of a significant number of publications [4-10]. Hydrogen bonds play a very important role in chemical reactivity, solvation, and most importantly the advancement of supramolecular chemistry, with the aim of designing and controlling crystal structures with interesting architectures. This goal has however remained elusive. The ability to understand and predict the formation of a hydrogen bond is of great importance to the chemical scientist [11-14].

Different functional groups containing some donor and acceptor groups including FH, OH, NH, SH, F, O, N, and S, as well as π -electrons, have been used as structure-directing motifs in different hydrogen-bonded structures [15-17]. Among these groups, the *N,N'*-disubstituted ureas have proven to be very reliable supramolecular building blocks due to their ability to form persistent one dimensional (1-D) α -tape hydrogen-bonded chains (**Figure 1**) in a variety of environments including solutions [18, 19], gels and fibers [20, 21], as well as in the solid-state [22, 23]. The *N,N'*-disubstituted ureas can act as both hydrogen bond donors through their two NH protons and acceptors through the lone pairs of the C=O group. The 1-D motifs in disubstituted ureas have been consistently exploited for the design of some fascinating hydrogen-bonded architectures [24-27].

Despite the exceptional ability of *N,N'*-disubstituted ureas to form highly robust crystalline solids of targeted architecture, there is still a limited level of reliability as the vast majority of the functional groups may assume alternative motifs in the solid-state depending on the presence of other competing functional groups or sterically bulky substituents [28]. The number of reports on the use of hydrogen bonding as a structure control element in crystal engineering and self-assembly of molecular structures is on the increase and scientists have continued to examine the connection between molecular perturbation and crystal packing in the solid-state [10]. However, understanding of how a functional group or alkyl chain modification will alter the

supramolecular architecture of a hydrogen-bonded structure is still evolving. Our interest in asymmetrically substituted urea compounds is as a result of the possibility of incorporating different functionalities to form designer compounds with interesting physical, chemical and biological properties. Here we illustrate the formation of unpredictable hydrogen-bonded motifs in some N,N' -disubstituted ureas containing carboxyl (COOH) and phosphoryl (P=O) functionalities and their structural, chemical and biological properties.

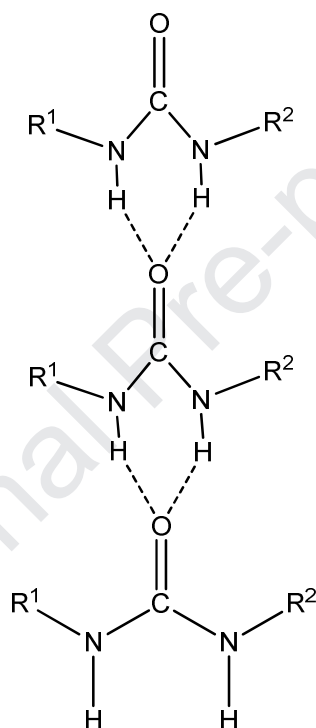


Figure 1: One-dimensional α -tape urea chain.

2. Experimental

2.1. General Experimental Methods

All chemicals were obtained from Sigma Aldrich and were used without further purification. Micro-analytical data were collected by the Campbell Microanalytical Laboratory, Department of Chemistry, University of Otago, New Zealand. ESI-mass spectra were recorded in positive ion mode on a Bruker MicrOTOF instrument in methanol. Infrared spectra were recorded as KBr

discs on a Perkin-Elmer Spectrum 100 Fourier Transform Infrared Spectrometer with a wavenumber range of 4000-400 cm^{-1} . $^{31}\text{P}\{^1\text{H}\}$ and ^1H NMR spectra were recorded on a Bruker Avance(III) 400 MHz NMR instrument in DMSO-d_6 or CDCl_3 at 300 K. Chemical shifts were quoted to external H_3PO_4 (^{31}P) and SiMe_4 (^1H). Melting points were recorded on a Reichert–Jung thermovar instrument as solid samples on glass slides.

2.2. X-ray crystallography

Diffraction data were collected at 100 K on an Agilent (Supernova, single source at offset Atlas) diffractometer equipped with an EOS CCD area detector and a 4-axis KAPPA goniometer. Graphite monochromated $\text{Cu-K}\alpha$ radiation ($\lambda=1.54184 \text{ \AA}$) was used. Data integration, scaling, and empirical absorption correction was carried out using the CrysAlis-Pro program package [29]. The structures were solved with intrinsic phasing method in ShelXT and refined by Matrix-least-square against F^2 . The non-hydrogen atoms were refined anisotropically, and hydrogen atoms were placed at idealized positions and refined using the riding model. All calculations were implemented in OLEX2 program package [30]. Important crystallographic and refinement parameters are presented in **Table 1**.

2.3. Quantum chemical methods

Quantum chemical calculations were carried out using the Gaussian 2009 program suite [31] on the University of Waikato's high-performance computing facility. Geometry optimizations and harmonic frequency calculations in the gas phase were completed with the B3LYP functional and repeated with the B3LYP-D3 by adding the keyword "empirical dispersion=gd3" and using the 6-311G++(d,p) basis set. The absence of imaginary frequencies in the calculated vibrational frequencies of the compounds showed that the optimized geometries were the true minima. Single point energy calculations at the B3LYP-D3 level of theory using 6-311G++(d,p) basis set were completed using the experimental crystal structures. Noncovalent interaction (NCI) analysis was undertaken on these single point electron densities using a locally developed program, Bonder, and visualized with graphics software; Visual Molecular Dynamics (VMD).

2.4. Synthesis and characterization of urea ligands

2.4.1. *N,N'*-(2-carboxyl phenyl)phenyl urea (*L*₁)

This compound was synthesized using a modified literature method [32]. A mixture of anthranilic acid (6.85 g, 0.05 mmol) and phenyl isocyanate (5.6 mL, 4.96 g, 0.05 mmol) were reacted in dry THF (50 mL) under reflux for 3 h. After cooling to room temperature, aqueous NH₄Cl (10 %, 200 mL) was added and the resulting precipitate was filtered off and washed with water (70 mL). The product was recrystallized from a water-ethanol mixture 1:3, 150 mL and dried overnight under vacuum. Yield (8.46 g, 73 %). Melting range: 190-193 °C. Elemental analysis: Calculated %; C, 65.40; H, 4.76; N, 11.17, Found%; C, 65.48; H, 4.71; N, 11.12. ESI-MS: *m/z* 255.08(69 %) [M-H]⁺, 511.17(100 %) [2M-H]⁺. ¹H NMR (400 MHz) DMSO-d₆, δ ppm: 10.35 (s, 1H; CO₂H), 9.75 (s, 1H; NH), 8.34 (d, 1H; NH; *J* = 5.6 Hz), 7.9-8.2 (m; 9H; Ar). ¹³C NMR (100 MHz): 169.87 (1C, COOH), 152.77 (1C; C=O), 142.68 (1C; C-N; Ar), 140.17 (1C; C-N; Ar), 134.15 (1C; Ar), 131.43 (1C; Ar), 129.15 (2C; Ar), 122.58 (1C; Ar), 121.3 (1C; Ar), 120.32 (1C; Ar), 119.26 (2C; Ar), 115.99 (1C; Ar). IR (cm⁻¹): 3301(br) νO-H, 3134(m) νN-H, 1664(s) νC=O, 1599(s) ν_sNH, 1584(m) νNH, 1415(s) ν_sC=C, 1277(m) ν_{as}NCN, 1173(s) ν_sC-N, 1044(m) νC=N.

2.4.2. Diethyl 4-(3-phenylureido)benzyl phosphonate (*L*₂)

To a mixture of diethyl 4-aminobenzyl-1-phosphonate (0.535 g, 0.0022 mol, 1 equiv) in diethyl ether (20 mL) was added phenyl isocyanate (0.30 mL, 0.0025 mol, 1 equiv) dropwise and refluxed with gentle heat until a white precipitate appeared. The filtered product was washed with diethyl ether (15 mL) and recrystallized from ethanol to give a colorless solid. This was dried overnight in a vacuum. Yield (0.62 g 83 %). Melting range: 150-154 °C. Elemental analysis: Calculated %; C 59.66, H 6.59, N 7.73. Found %; C 59.61, H 6.31, N 7.68. ESI-MS, *m/z* 385.12(100%) [M+Na]⁺, 747.25(14.31%) [2M+Na]⁺, 1109.30(5.25%), [3M+Na]⁺. ¹H NMR (400 MHz) CDCl₃, δ ppm: 8.54 (s, 1H; NH), 8.12 (s, 1H; NH), 7.4-7.0 (m, 9H; Ar), 4.1 (m, 4H; CH₂, ester), 3.17 (d, 2H; CH₂, *J* = 8.6 Hz), 1.34 (t, 6H; CH₃, *J* = 8.2 Hz). ¹³C NMR (100 MHz) CDCl₃: 153.58 (s, C=O), 139.66 (s, C-N; Ar), 138.4 (s, C-N; Ar), 129.91 (d, 2C; Ar), 128.84 (s, 2C; Ar), 123.81 (s, 1C; Ar), 122.26 (s, 1C; Ar), 120.03 (d, 2C; Ar), 118.84 (s, 2C; Ar), 62.81 (d,

2C; CH₂), 32.38 (d, 1C; CH₂), 16.45 (d, 2C; CH₃). ³¹P{¹H} NMR: 27.80 (s). IR (cm⁻¹); 3346(br) νO-H, 3200(s) νN-H, 1708(s) νC=O, 1233(s) νP=O, 1029(s) νC=N, 976(s) νP-OR.

Table 1: Crystal data and structure refinement parameters for urea ligands L₁ and L₂

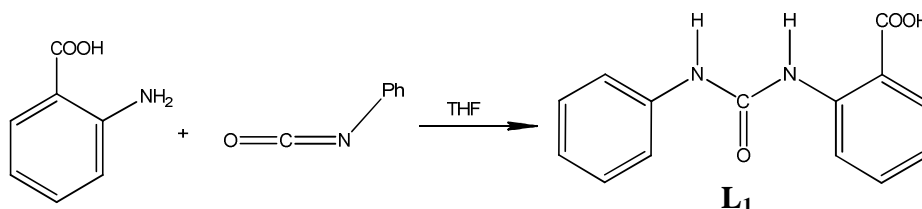
	L ₁	L ₂
Empirical formula	C ₁₄ H ₁₂ N ₂ O ₃	C ₁₈ H ₂₁ N ₂ O ₄ P
Formula weight	256.26	360.34
Temperature/K	100.00(10)	99.98(11)
Crystal system	monoclinic	monoclinic
Space group	P2 ₁ /n	P2 ₁ /n
a/Å	11.3928(3)	10.91600(10)
b/Å	4.8487(10)	11.35370(10)
c/Å	22.1770(5)	29.6292(2)
β/°	96.467(2)	98.9670(10)
Volume/Å ³	1217.27(5)	3627.27(5)
Z	4	8
ρ _{calc} /cm ³	1.398	1.320
μ/mm ⁻¹	0.830	1.560
F(000)	536.0	1520.0
Crystal size/mm ³	0.1072 × 0.0873 × 0.0603	0.1173 × 0.0955 × 0.0336
Radiation	CuKα (λ = 1.54184 Å)	CuKα (λ = 1.54184 Å)
2θ range for data collection/°	8.02 to 147.48	6.04 to 147.986
Index ranges	-14 ≤ h ≤ 13, -5 ≤ k ≤ 5, -27 ≤ l ≤ 19	-13 ≤ h ≤ 12, -13 ≤ k ≤ 14, -36 ≤ l ≤ 36
Reflections collected	4687	34555
Independent reflections	2336 [R _{int} = 0.0138, R _{sigma} = 0.0196]	7266 [R _{int} = 0.0292, R _{sigma} = 0.0242]
Data/restraints/parameters	2336/0/173	7266/0/454
Goodness-of-fit on F ²	1.073	1.058
Final R indexes [I ≥ 2σ (I)]	R ₁ = 0.0349, wR ₂ = 0.0836	R ₁ = 0.0583, wR ₂ = 0.1492
Final R indexes [all data]	R ₁ = 0.0404, wR ₂ = 0.0882	R ₁ = 0.0726, wR ₂ = 0.1569
Largest diff. peak/hole / e Å ⁻³	0.22/-0.21	1.52/-0.88

3. RESULTS AND DISCUSSION

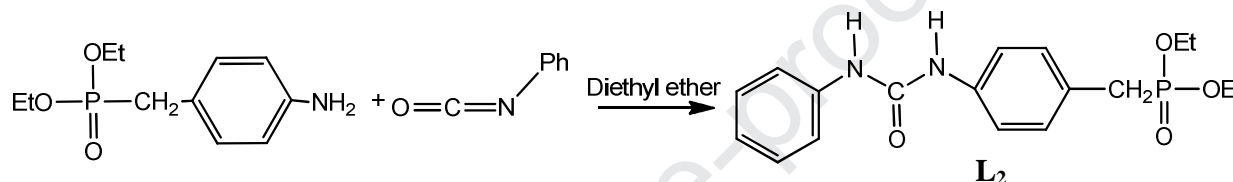
3.1. Synthesis and characterization

The ureas L₁ and L₂ (**Scheme 1 and 2**) were synthesized by the reaction of the corresponding amines and phenyl isocyanate in refluxing tetrahydrofuran and diethyl ether respectively. The insoluble product precipitated out of the solution on cooling. The products were recrystallized

from a 1:3 water-ethanol mixture for **L**₁ and ethanol for **L**₂. The compounds **L**₁ and **L**₂ have been synthesized previously [32, 33]; however, there are no reports on the chemical or structural characterization of both compounds in the literature.



Scheme 1: Reaction scheme for the synthesis of *N,N'*-(2-carboxyl phenyl)phenyl urea (**L**₁)



Scheme 2: Reaction scheme for the synthesis of *diethyl 4-(3-phenylureido)benzyl phosphonate* (**L**₂)

ESI-mass spectra of the carboxyphenyl-substituted urea **L**₁ (**Figure S1** of the supplementary information) in methanol solution and negative ion mode showed pseudo molecular ion peaks at m/z 255.08 and 511.17 for $[M-H]^+$ and $[2M-H]^+$ respectively. The spectrum for the phosphoryl-substituted urea **L**₂ showed an ion at m/z 385.12 for the sodium adduct of the compound. Addition of two drops of NaCl solution to the analyte solution resulted in a very intense peak for the sodium adduct. Two other molecular ion peaks were observed in the spectra at m/z 747.25 and 1109.30 corresponding to $[2M+Na]^+$ and $[3M+Na]^+$.

In the ¹H NMR spectra of the compounds, **L**₁ (**Figure S2**) showed a singlet at 10.35 ppm resulting from the carboxyl proton. Singlet peaks appeared at 9.75 and 8.35 ppm corresponding to the two NH protons of the urea. The phenyl ring protons were observed as multiplets at 7.9–8.5 ppm. The more downfield NH proton of **L**₁ is probably as a result of intramolecular hydrogen bonding as evident in the crystal structure of the compound. The phosphoryl substituted urea **L**₂ (**Figure S3**) showed singlets 8.54 and 8.12 ppm for the two NH protons and a multiplet at 7.4 ppm corresponding to the phenyl protons in the compound. Another multiplet observed at 4.1 ppm corresponds to the POCH₂ protons of the phosphoryl ester. The spectra also showed a

doublet at 3.17 ppm resulting from the protons of the PCH₂ group. The triplet at 1.34 ppm is from the methyl groups of the phosphoryl ester.

The ¹³C NMR of the urea **L**₁ (**Figure S4**) recorded in DMSO-d₆ showed a carboxyl carbon peak at 169.87 ppm and carbonyl carbon peak appearing at 152.77 ppm. Similar chemical shifts were reported for urylene dicarboxylic acids [34]. The peaks at 142.68 and 140.17 ppm correspond to the phenyl carbons bonded to the urea nitrogen. The peaks are further downfield than the other phenyl carbon peaks due to the deshielding effect of the urea nitrogen bonded to it. The peaks around 134.55–115.99 ppm are from the remaining phenyl carbons of the urea. The ¹³C{¹H} NMR spectrum of **L**₂ was similar to **L**₁ and also presented in the supplementary information (**Figure S5**). The peak at 153.58 ppm corresponds to the urea carbonyl carbon while the peaks at 139.66 and 138.4 ppm are as a result of the urea nitrogen bonded carbons. The peaks appearing around 129.91–118.84 ppm correspond to the other phenyl carbons in the compound. The doublet at 62.8 ppm is for the two CH₂ carbons of the phosphoryl ester. The doublet is presumably due to P-C coupling. These peaks are further downfield than the peaks for the bridging PCH₂ carbon (32.38 ppm) due to the electron-withdrawing effect of the phosphoryl oxygens. The doublet at 16.45 ppm is a result of the two methyl protons of the phosphoryl ester. The ³¹P{¹H} NMR spectrum of **L**₂ (**Figure S6**) shows a singlet at 27.8 ppm corresponding to the PO₃Et₂ phosphorus.

The infrared spectra of **L**₁ and **L**₂ (**Figures S7 and S8**) show stretching frequencies at 3301 cm⁻¹ for the carboxyl OH in **L**₁. The carbonyl stretching frequencies appear at 1664 cm⁻¹ and 1708 cm⁻¹ for **L**₁ and **L**₂ respectively. The N-H stretching frequencies appear around 3200 - 3100 cm⁻¹ for both **L**₁ and **L**₂ and the P=O stretching frequency was observed as an intense peak at 1232 cm⁻¹ for **L**₂.

3.2. Structural Analysis

3.2.1. *N,N'*-(2-carboxyl phenyl)phenyl urea (**L**₁)

The compound **L**₁ crystallized in a centrosymmetric monoclinic crystal system and P2₁/n space group. The molecular structure of the compound is shown in **Figure 2**, and selected bond lengths and angles are presented in **Table 2**. The core of the urea structure is essentially planar with the COOH functional group twisted out of the plane of the adjacent urea by a torsion angle of 41.26° defined by C1-N2-C2-C3. The urea carbonyl oxygen is also slightly out of the plane of

the urea functional group with a torsion angle of 9.68° defined by the torsion angle involving atoms O1-C1-N1-C9. The hydrogen-bonded structure of the compound (**Figure 3**) shows a complex interplay of intra and intermolecular hydrogen bonding. There is strong intramolecular hydrogen bonding between the carboxylic acid group and the adjacent urea N-H. Ureas are known to form 1-D bifurcated hydrogen bonds between the two N-H donors of the urea and the lone pairs on the carbonyl oxygen of a second molecule of the urea [35]. These urea N-H \cdots O bonds are reported to be so strong that they can persist even in the presence of other strong hydrogen bond donor groups[36]. However, the presence of carboxylic acid groups on the adjacent phenyl of the *N,N'*-disubstituted urea **L**₁ probably initiated some competition between the different functional groups in the crystal lattice. This competition must have resulted in the rearrangement of the hydrogen bonding architecture of the urea ligand from the usual bifurcated one-dimensional α -network of bonds to a two-dimensional hydrogen-bonded chain (**Figure 4**).

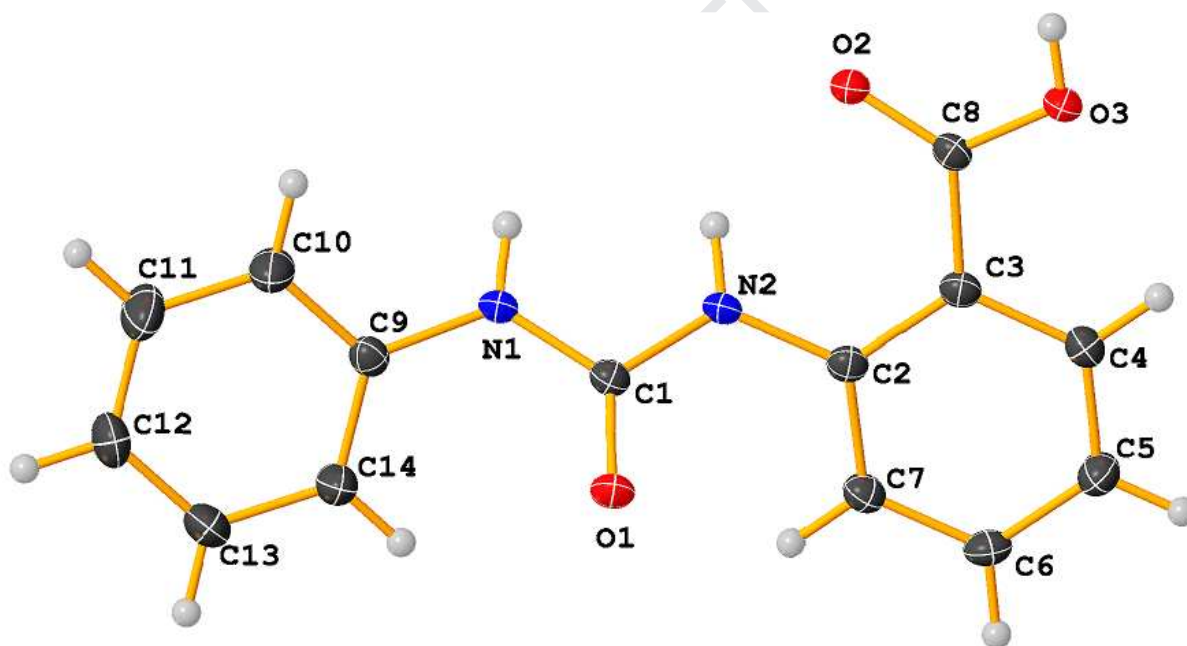


Figure 2: Molecular structure of the *N,N'*-(2-carboxyl phenyl)phenyl urea **L**₁. Ellipsoids are drawn at 50% probability.

The 2-D hydrogen-bonded structure consists of three distinct hydrogen bonding interactions which include: **i.** Intramolecular hydrogen bond interaction between the carboxylic acid acceptor functional group and one of the urea nitrogen donors, **ii.** a linear α -tape inter-

molecular hydrogen bond interaction between the second N-H donor and the urea carbonyl acceptor group and **iii.** a hydrogen-bonded dimer between the carboxylic acid functional group and another molecule containing the carboxylic acid moiety. The hydrogen bond distances and angles are presented in **Table S1** of the supplementary information, shows that the intramolecular bond distances between the urea nitrogen and the oxygen of the carboxylate (N2-O2 = 2.683Å) are shorter than the intermolecular NH \cdots O bond length of 2.876Å which is comparable to the average N-H \cdots O hydrogen bond distance of 2.85Å [27]. The proximity of the competing carboxylic acid group to the urea N-H-donor group is probably the reason for the strong intramolecular hydrogen bond between the urea N-H functional group and one of the carboxyl oxygens (O2) orthogonal to the N-H-donor group. These intra-molecular hydrogen bonds tend to have disrupted the usual bifurcated α -tape hydrogen bond chain usually observed in *N,N'*-substituted ureas of this kind. The carboxyl group also forms a hydrogen-bonded dimer with a second molecule through the carboxylic acid functional group. The relatively strong intermolecular CH \cdots O hydrogen bond has a rather short bond distance (DHA 2.581Å) and an almost linear hydrogen bond angle (\angle DHA =173°).

The second urea N-H-donor group forms a continuous linear chain of hydrogen bonds with the carbonyl oxygen of a second molecule of the urea, resulting in an array of unexpected 2-D hydrogen-bond motifs (**Figure S9**) held together by intramolecular hydrogen bond and stabilized by intramolecular and inter-molecular C-H \cdots O and NH \cdots O interactions in the crystal lattice (**Figure 4**). Related compounds exhibiting self-complementary hydrogen bonds between urea and carboxyl groups were reported by Zhao *et al.* [34].

Table 2 : Selected bond lengths and angles for ureas L₁ and L₂

Bond Lengths (Å)		Bond Angles (°)	
L₁			
O2 – C8	1.2366(17)	C9 – N2 – C1	125.17(12)
O3 – C8	1.3141(16)	C2 – N1 – C1	124.34(12)
O1 – C1	1.2295(17)	O3 – C8 – O2	122.61(12)
N2 – C1	1.3580(18)	C7 – C8 – O2	123.24(12)
N2 – C9	1.4215(17)	C7 – C8 – C3	114.15(11)
N1 – C1	1.3834(17)	N2 – C1 – O1	124.13(12)
N1 – C2	1.3994(17)	N1 – C1 – N2	113.21(12)
C3 – C4	1.382(2)	C3 – C2 – N1	120.63(12)
L₂			
P1A – O3A	1.5785(18)	O3A – P1A – C14A	103.88(11)
P1A – O4A	1.5710(17)	O4A – P1A – O3A	106.96(10)
P1A – O2A	1.4741(18)	O4A – P1A – C14A	108.17(10)
P1A – C14A	1.789(2)	O2A – P1A – O3A	113.92(10)
P1B – O3B	1.565(3)	O2A – P1A – O4A	108.63(10)
P1B – O2B	1.456(2)	O2A – P1A – C14A	114.86(11)
P1B – O4B	1.601(3)	O3A – P1B – O4B	102.43(15)
P1B – C14B	1.792(3)	O2B – P1B – C14B	104.02(13)
O3A – C17A	1.462(3)	O2B – P1B – O3B	115.60(17)
O4A – C15A	1.456(3)	O2B – P1A – O4B	114.43(14)
O1B – C1B	1.220(3)	O2B – P1B – C14B	116.26(15)
O1A – C1A	1.219(3)	O4B – P1B – C14B	102.23(15)
N1B – C8B	1.404(3)	C17A – O3A – P1A	122.64(17)
N1B – C1B	1.376(3)	C15A – O4A – P1A	123.73(15)
N1A – C2A	1.408(3)	C1B – N1B – C8B	128.5(2)
N1A – C1A	1.372(3)	C1A – N1A – C2A	128.1(2)
N2B – C1B	1.375(3)	C1B – N2B – C2B	128.8(2)
N2B – C2B	1.399(3)	C1A – N2A – C8A	128.1(2)
N2A – C1A	1.367(3)	C15B – O3B – P1B	124.2(2)
N2A – C8A	1.409(3)	C17 – O4B – P1B	126.0(3)

Note: A and B refer to two independent molecules

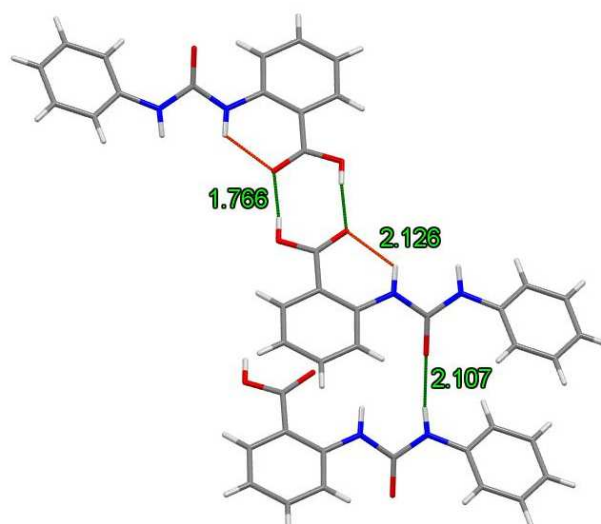


Figure 3: Interplay of inter and intra-molecular hydrogen bonding in the structure of L_1 . The intramolecular bonds are shown in red while the intermolecular bonds are green in color. The relative proximity of the carboxyl oxygen to the urea NH contributes to the distortion of the usual α -tape synthon prevalent in di-substituted ureas.

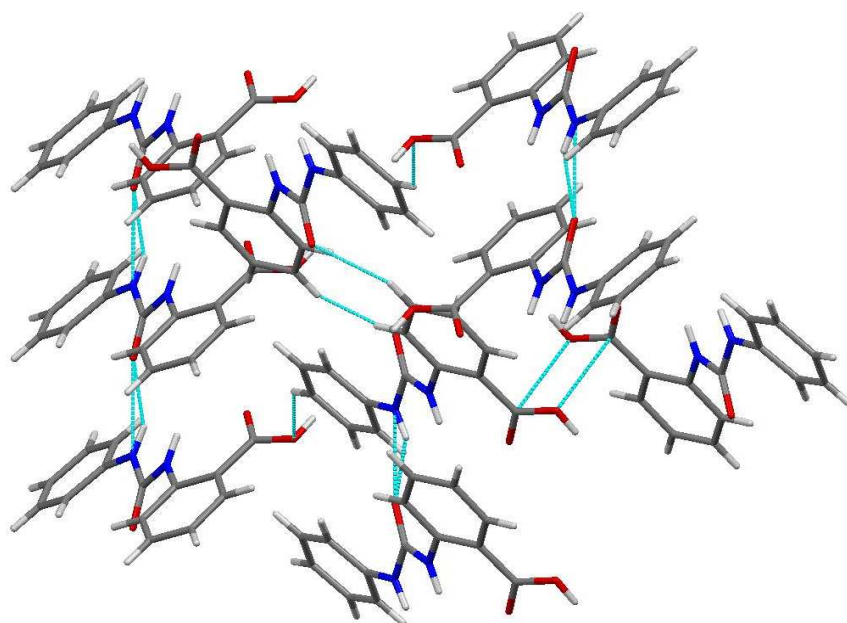


Figure 4: Intermolecular CH...OH and NH...O=C stabilizing interactions in the hydrogen-bonded structure of L_1 .

3.2.2. Diethyl 4-(3-phenylureido)benzylphosphonate (L_2)

The phosphoryl ester functionalized urea (L_2) crystallized in a centrosymmetric $P2_1/n$ crystal system. The crystal structure of the compound showed the presence of two similar but distinctively different molecules in the asymmetric unit. The molecular structures of the two molecules are labeled (**A**) and (**B**) (**Figure 5**) and selected bond lengths and angles are presented in **Table 2**. The crystal structure of molecule **B** showed a disorder on one of the ethyl groups of the phosphoryl ester, which was modeled in two positions and a constraint introduced to stabilize the molecule. Only one position is shown in **Figure 5** for clarity. The structures of the compounds show significant differences in the orientations of the substituted phosphoryl ester. The two POEt groups in the molecule (**A**) are pointed in opposite directions with one of the groups oriented towards the adjacent phenyl ring. In the second molecule (**B**), the POEt groups are pointed in the same direction and away from the adjacent phenyl ring. Also, in the molecule (**A**), P=O points in the opposite direction to the C=O, but in the same direction in the molecule (**B**). These differences in geometric orientation of the structures also result in slight differences in the bond distances and angles of the two structures. For example, the P1-O3 bond has a bond length of 1.5785(18) Å in (**A**) and 1.5665(3) Å in (**B**), while the O4-P1-C14 angle in (**A**) is 108.17(10)° and that in (**B**) is 102.23(15)°. Even though there was a slight disorder in one of the ethyl carbons of the phosphoryl ester group of the structure (**B**), the overall structure of the urea was preserved. The two molecules are linked by the bifurcated hydrogen bonds between the phosphoryl oxygen of one molecule and the two N-H-donor groups of the second molecule. The two molecules then form one bifurcated hydrogen bond with each of the two molecules of the urea, resulting in a hydrogen-bonded tetramer (**Figure 6**). The urea tetramer shows two different bifurcated hydrogen bonds at each end of the molecule. The following hydrogen bond distances and angles, [2.924 Å; 156°; N(1A)-H(1A)-O(2B), 2.837 Å; 162°; N(2A)-H(2A)-O(2B)] and [2.870 Å; 160°; N(1B)-H(1B)-O(2A), 2.843 Å; 158°; N(2B)-H(2B)-O(2A)] were recorded for the two different hydrogen bonding interactions observed in the tetramer. The tendency for urea compounds to form 1-D hydrogen-bonded chains using the two NH proton donors and the carbonyl proton acceptor in a bifurcated hydrogen bond motif according to Etter *et al.* [37] comes from the linear mode of approach of the N-H donors to the lone pairs on the C=O hydrogen bond acceptor. This process is however disrupted by the presence of a competing phosphonate hydrogen bond acceptor, resulting in the rearrangement of the predicted hydrogen

bonding architecture of the urea in the crystal lattice. This rearrangement is predicted to be the reason for the formation of a chain of bifurcated hydrogen-bonded tetramers shown in **Figure 6**.

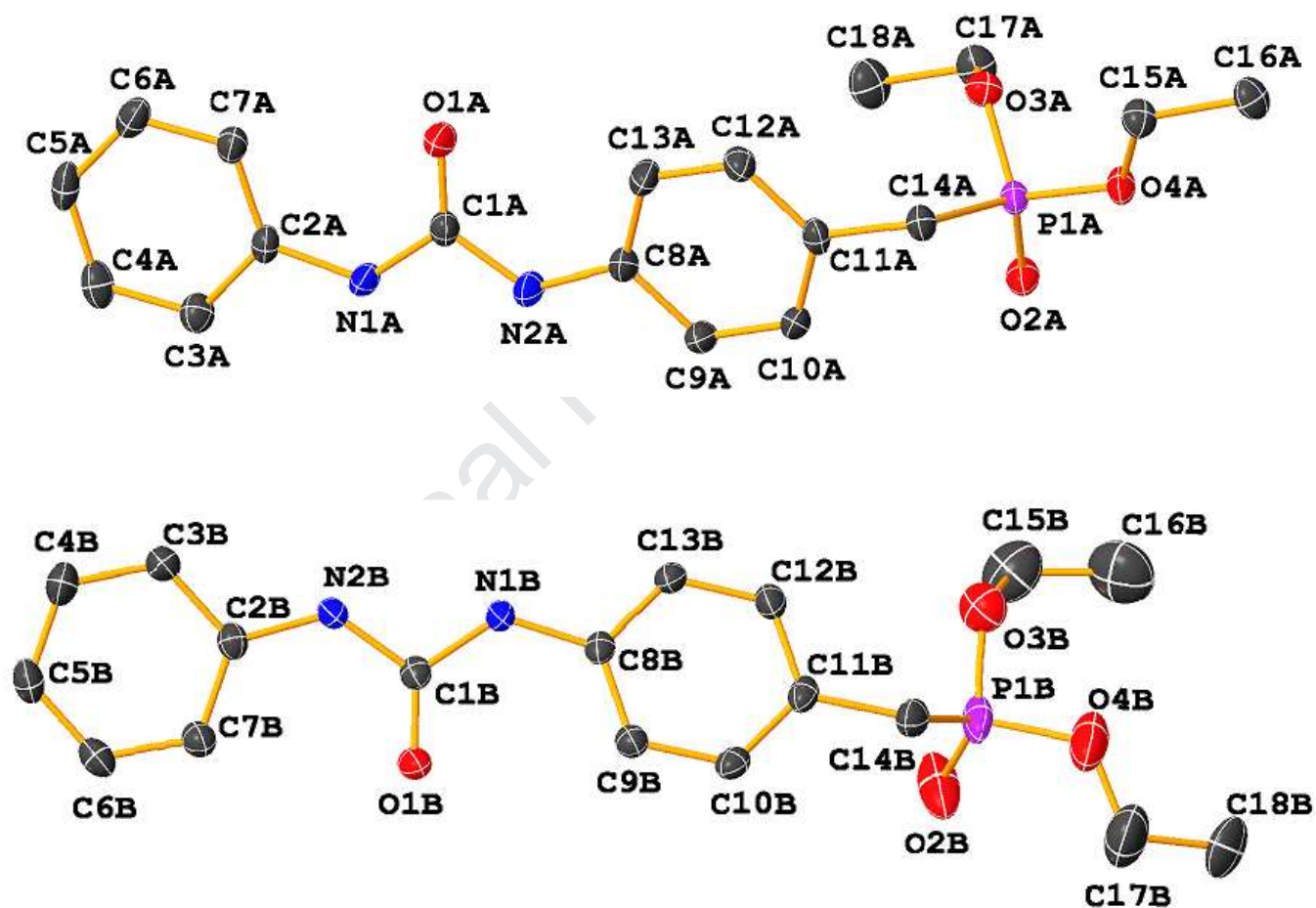


Figure 5: Molecular structure of L₂ showing two independent molecules in the asymmetric unit.

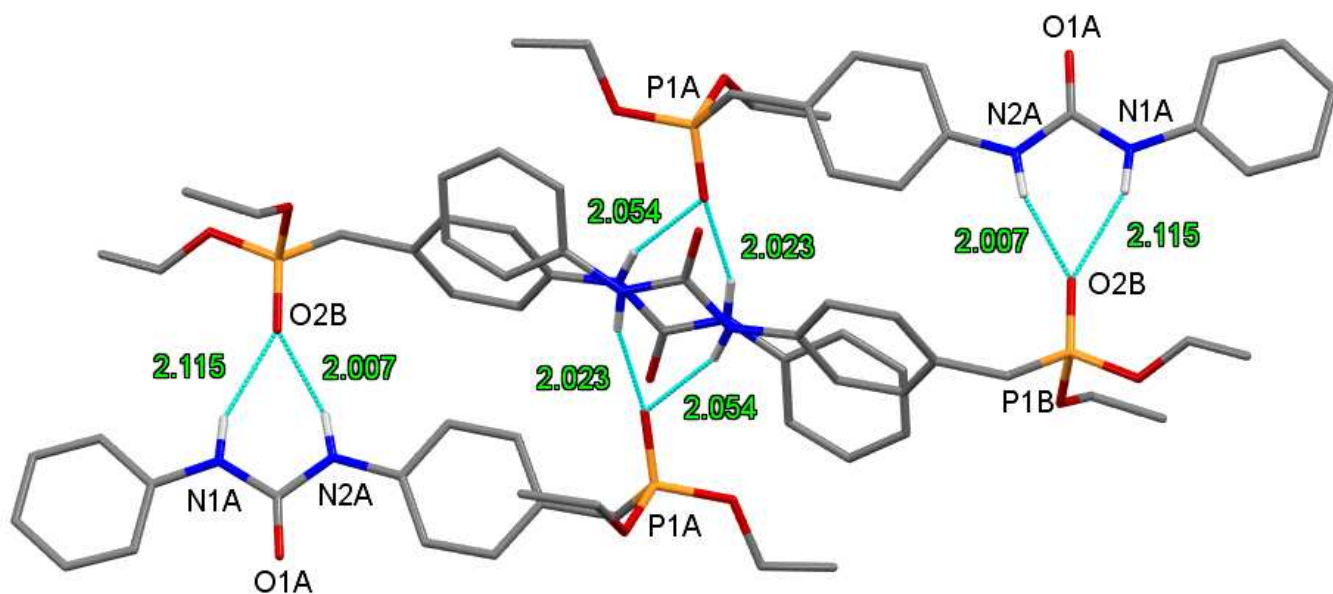


Figure 6: A side view of the hydrogen-bonded tetramer of L_2 showing different hydrogen bond distances at each end of the tetramer.

3.4. Non-covalent interactions

Due to the rich and challenging bonding patterns in crystalline solids, it can be difficult to experimentally rationalize the different bonding distributions in crystalline compounds, especially those exhibiting various degrees of non-covalent interactions. Consequently, researchers have increasingly turned to various theoretical approaches to investigate the nature and strength of non-covalent interactions. A number of these are based on topological analysis of the electron density [38-41], including the Electron Localization Function (ELF) [42], the Quantum Theory of Atoms in Molecules (QTAIM) [43] and most recently the Non-Covalent Interaction index (NCI) [44]. The NCI theory is based on the reduced density gradient(s),

$$s = \frac{1}{2(3\pi^2)^{1/3}} \frac{|\nabla\rho|}{\rho(\mathbf{r})^{4/3}} \quad 1$$

A combination of the reduced density s and the density ρ allows a spatial representation of bonding regions in real space. Regions of high reduced density and low density correspond to non-interacting density tails, while regions of low reduced density and low density correspond to

noncovalent interactions. The different types of interactions can now be distinguished by plotting the sign of the second eigenvalue λ_2 as the ordinate against the reduced density gradient $s(\rho)$. Analysis of the sign of λ_2 thus helps to ascertain the different types of weak interactions and whether these are attractive or repulsive, whereas the density itself provides information about the strength of the interactions. Attractive non-covalent interactions are associated with regions where the electron density is domiciled with respect to the plane perpendicular to the bond path and have values of ($\lambda_2 < 0$) while repulsive non-covalent interactions appear at values of ($\lambda_2 > 0$)[45, 46].

The non-covalent interactions of disubstituted ureas **L₁** and **L₂** were investigated with a locally-developed program, Bonder, which provides numerically equivalent results to existing NCI codes such as NCIPLOT, NCImilano or MultifwN. However, Bonder offers some advantages to these existing codes, particularly for larger molecules, in that it analyzes each discrete non-covalent interaction separately, rather than constructing a single sparse matrix, including the many regions where there are not non-covalent interactions. Input geometries were taken from the crystal structures of the ligands, and the wave functions files were generated at the DFT level of theory using the B3LYP-D3 functional and the 6-311++G(d,p)** basis set.

In order to unambiguously characterize interactions from the two main competing groups in the hydrogen-bonded structure of the carboxyl-substituted urea **L₁**, the NCI analysis of this compound was performed in two parts. The 2-D electron density plots and 3-D isosurface troughs for the carboxylic acid dimer end of the structure are presented in **Figure 7**. The 2D-plots and their corresponding 3D isosurface representation indicate the presence of the three main categories of interactions. The first is the very strong intermolecular hydrogen bonding interactions in the carboxylic acid dimer shown as a deep blue peaks at the far end of the $\text{sign}\lambda_2$ axis with a density value of $\rho = 0.47$ and $\lambda_2 < 0$ (**Figure 7a**). The high ρ value of this interaction is indicative of very strong attractive hydrogen bonding interaction and corresponds to two deep blue compact pill-shaped isosurface volumes between the two carboxylic acid groups in the 3-D isosurface plot, **Figure 7b**. There are also the green isosurface volumes between the two blue isosurfaces corresponding to weak non-bonding van der Waal interactions between the adjacent carboxylic acid hydrogens. This weak interaction corresponds to the peaks at critical density value $\rho = 0.009$ a.u. and $\lambda_2 > 0$ in the 2-D plot.

The second set of interactions in the urea dimer are the benzene ring closure interactions which are at the positive end of the 2-D plot with a reddish-green trough at a density value of $\rho = 0.023$ a.u. and $\lambda_2 > 0$ corresponding to red cigar-shaped isosurfaces at the center of the benzene rings. These red-colored isosurfaces are as a result of steric interactions within the benzene ring. The third and final set of interactions that observed in the dimer are the intra-molecular interactions, including the NH---OC intramolecular hydrogen bonding interactions and the weak CH---OC intramolecular interactions. The NH---OC intramolecular hydrogen bonding interaction between the urea NH functional group and one of the carboxylic oxygens appears as a low density, low gradient deep blue peak ($\rho = 0.38$ a.u. a.u. and $\lambda_2 < 0$) on 2-D plot and characteristic of strong intramolecular hydrogen bonding [46]. The 3-D isosurface ($s = 0.5$) indicated by a round blue pill-shaped trough and a reddish-green almond-shaped trough. The blue isosurface area represents the directional attractive intramolecular hydrogen bonding interaction between the carboxyl O acceptor and the N-H donor, corresponding to the low s and low $\rho = 0.038$ a.u. and $\lambda_2 < 0$ on the 2-D electron density plot. The reddish-green almond-shaped isosurface results from some steric crowding within the five-membered ring formed by the intramolecular hydrogen bond interaction [47]. This steric interaction corresponds low s and low ρ peak of the 2-D electron density plot with $\rho = -0.020$ a.u. and $\lambda_2 > 0$. The weaker intramolecular CH---OC interactions are represented by the symmetric peaks at $\rho = 0.020$ a.u. and -0.015 a.u. on both sides of the $\text{sign}\lambda_2$ axis of the 2-D electron density plot respectively. These interactions correspond to the bi-centric stabilizing blue end of the flat isosurface and the multi-centric non-stabilizing end of the isosurface resulting from the strain inside the five-membered ring formed by the interaction. Similar symmetric interactions has been reported for intra-molecular CH---OC interactions in *N*-acetyl-phenylalanyl-amide (NAPA) [47], and *N,N*-diethyl-*N'*-palmitoyl thiourea [48].

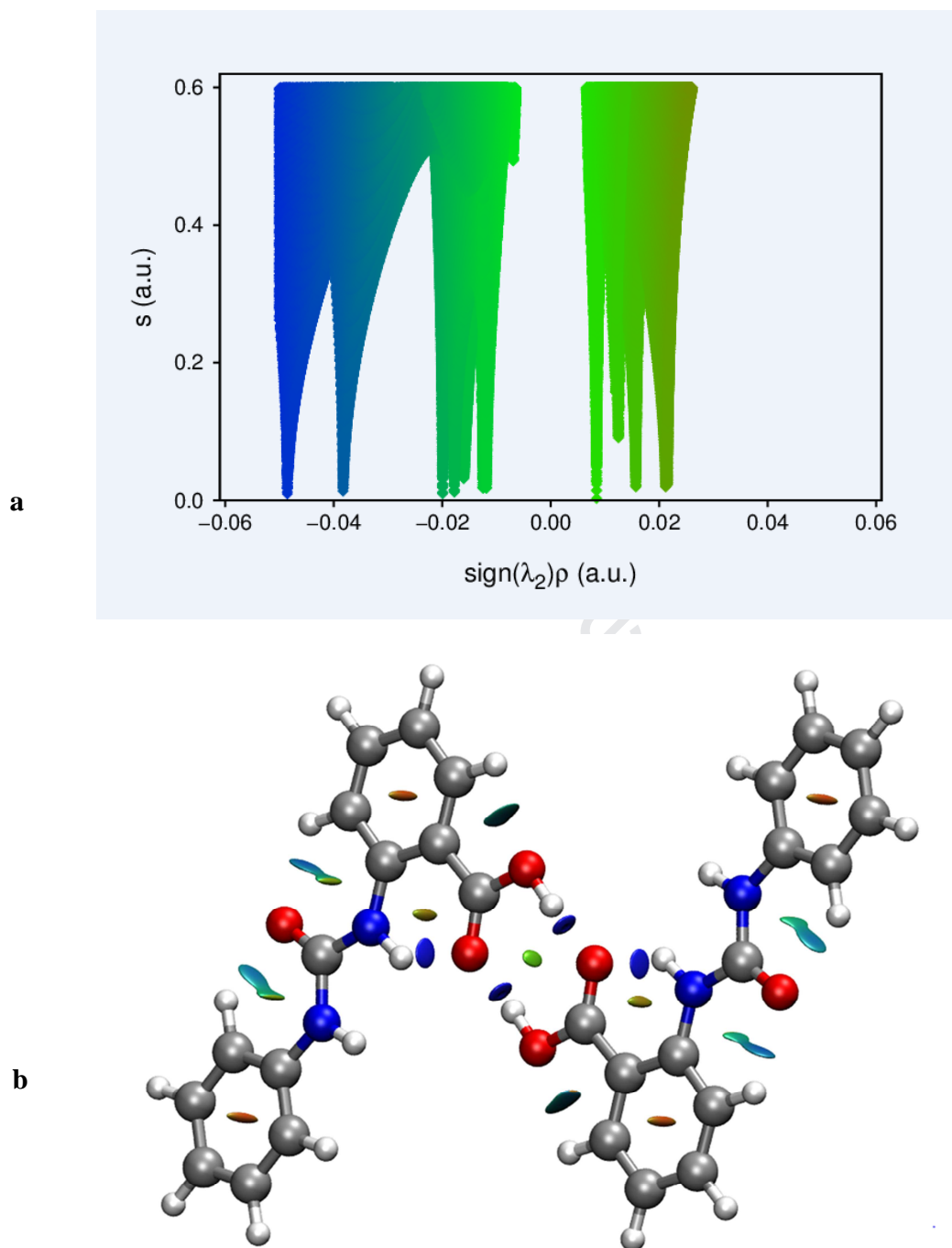


Figure 7: (a) The plot of the reduced density gradient (s) against $\text{sign}\lambda(\rho)$ for the COOH dimer in the crystal structure of urea ligand \mathbf{L}_1 . (b) Gradient isosurface representation for carboxylic acid dimer ($s=0.5$). The surfaces are scaled in blue, green and red coloration according to the $\text{sign}(\lambda_2)\rho$, from -0.2 to 0.2 a.u. Blue indicates strong, attractive interactions, and red indicates strong repulsive interactions or steric clashes.

The primary interaction in the second part of the hydrogen-bonded urea **L₁** is the α -urea tape N-H---O-C intermolecular hydrogen bonding. A separate 2-D electron density plot shows a bluish-green peak with $\rho = 0.018$ a.u. from a strong stabilizing intermolecular hydrogen bond interaction and corresponding to the single blue pill-like isosurface volume between the N-H donor and the carbonyl acceptor functional group of another molecule of the ligand (**Figure S10**). The value of ρ for this interaction is slightly less negative than the density value for the intramolecular NH---OC interaction found in the first part of the structure (**Figure 7**), which indicates a higher stabilizing effect for the intramolecular hydrogen bonding interaction relative the intermolecular hydrogen bonding interaction. This explains the distortion of the usual α -tape hydrogen bonding architecture of the urea to form a 2-D supramolecular structure.

The 2-D plots and the corresponding isosurface troughs for the urea ligand **L₂** are presented in **Figure 8**. The first interaction in order of strength is the strong intermolecular hydrogen bonding interaction between the lone pairs on the phosphoryl oxygen and the NH protons of the urea functional group. The peaks at $\rho = 0.022$ a.u.; $\lambda_2 < 0$ in the 2-D electron density plot corresponding to dark blue pill-like isosurface volumes on the right-hand side of the 3-D isosurface representation. Another peak directly to the right of the first one with $\rho = 0.018$ a.u. and $\lambda_2 < 0$ is for the second intermolecular hydrogen bonding interaction in the bifurcated arrangement and corresponds to the second pill-like isosurface on the right-hand side of the 3D plot and attached to the little bluish-green isosurface volume. The bluish-green isosurface trough between the two pill-like volumes is a result of some weak van der Waals interaction between the two adjacent hydrogens of the urea with $\rho = 0.01$ a.u. and the red tint on the green isosurface must have resulted from multicentric repulsive interactions within the four-membered ring formed by the urea nitrogens and carbonyl carbon. At the other end of the 2D electron density plots with $\rho = 0.02$ a.u. ; $\lambda_2 > 0$ is a reddish-green peak indicative of strong repulsive or steric interaction and corresponds to the red-isosurface volumes at the center of the benzene rings in the dimer.

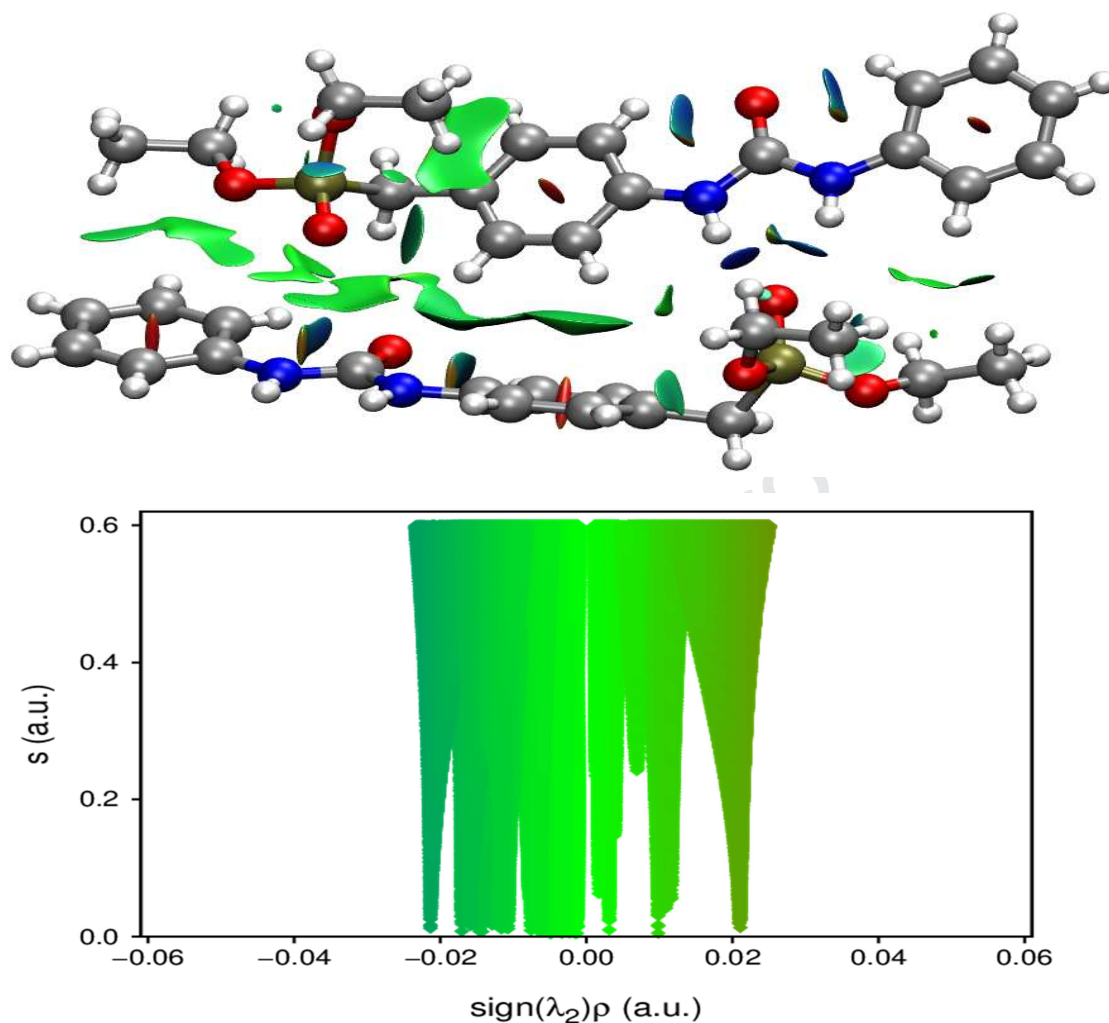


Figure 8: The 2-D electron density plots for the phosphoryl urea dimer (top) and the corresponding 3-D isosurface representations (bottom) ($s = 0.5$ a.u.) ($-0.05 < \rho < 0.05$ a.u.).

These red isosurface volumes at the center of the benzene rings are a result of strong multicentric steric repulsion within the benzene ring. Apart from the strong, attractive hydrogen bonding interactions between the phosphoryl oxygen acceptor and the urea N-H donors, there is also the presence of strong, attractive non-bonding CH----OC interactions. The two almond-shaped bicolored (blue/red) isosurfaces depict some fairly strong attractive interactions with critical density values of $\rho = 0.017$ a.u. representing some bicentric directional stabilizing interaction between the phenyl carbons on each side of the carbonyl group and the carbonyl oxygen. The red lower end of the isosurface is a result of a strain in the five-membered ring

formed by the interaction due to the multicentric nature of the density around the ring backbone. This interaction corresponds to the peaks on the 2D Bonder plot with $\rho = 0.015$ a.u. and $\lambda_2 > 0$; characteristic of ring closure interactions [46]. Similar interactions were reported for 2-([2-(phenylsulfonyl)hydrazinylidene]methyl)benzoic acid [49].

3.6. Molecular Docking

The synthesized compounds **L**₁ and **L**₂ were studied for their binding affinities through molecular docking against specific proteins implicated in cancer. The two proteins used are epidermal growth factor receptor kinase - EGFR kinase (PDB code: 2J5F) and anaplastic lymphoma kinase - ALK (PDB code: 5J7H). EGFRs are a large family of receptor tyrosine kinases (TK), which are one of the main tumor makers in many types of cancer [50]. They are expressed in different types of cancer, including breast, lung, oesophageal, head, and neck [51]. They play critical roles in the complex, signaling cascade that modulates growth, differentiation, adhesion, migration, and survival of cancer cells. Owing to the multidimensional roles they play in the progression of cancer, EGFR, and its family members have emerged as attractive candidates for anti-cancer therapy [52]. Specifically, the aberrant activity of EGFR has been associated with cellular proliferation and apoptosis, resulting in the development and growth of tumor cells [53]. The increasing knowledge of the structure of EGFR has provided the impetus for focused-oriented development of new anticancer chemotherapies.

ALK regulates the development and maintenance of the nervous system. Detailed studies by Griffin *et al.*, 1999 and Gascoyne *et al.*, 2003 revealed that ALK fusion genes were drivers of inflammatory myofibroblastic tumors and diffuse large B-cell lymphoma [54, 55]. Also, the amplification or activating point mutations of the ALK gene have been reported in neuroblastoma [56], anaplastic thyroid cancer [57], and ovarian cancer [58]. The use of ALK as oncogenic drug target was further amplified when a novel fusion gene involving ALK and the echinoderm microtubule-associated protein-like 4 (EML4) gene was identified in approximately 5% of non-small-cell lung cancer (NSCLC) [59], independent of other oncogenic driver mutations like (EGFR) or Kirsten rat sarcoma virus (KRAS) mutations. In the US, new cases of ALK+ lung cancer are estimated to exceed 8000 per year. This finding has made ALK a valid molecular target, especially for NSCLC patients.

The solubility and binding modes of substituted urea compounds containing carboxyl and phosphoryl acceptor functionalities, **L**₁ and **L**₂ were calculated and compared with the results for *N,N'*-diphenylurea without carboxyl and phosphoryl functional groups **L**₃, (**Figure S11**). The docking protocols were validated, and the results are presented in **Figure S12**.

Table 3: Binding energy of the synthesized compounds in the drug targets, 2J5F and 5J7H

Drug target: 2J5F			Drug target: 5J7H	
	London dG	GBV/WSA dG	London dG	GBV/WSA dG
<i>Comp</i>	ΔG (kJ/mol)	ΔG (kJ/mol)	ΔG (kJ/mol)	ΔG (kJ/mol)
L ₁	-44	-25	-44	-22
L ₂	-46	-27	-51	-23
L ₃	-35	-19	-34	-16
Native ligand	-46	-28	-56	-33
Doxorubicin	-65	-29	-75	-31

The presence of the carboxylate and the phosphonate ester groups did not significantly affect the aqueous solubility of the compounds (**Table S1**). Likewise, the partition coefficient was within the range as prescribed by Lipinski's rule of five ($\log P \leq 5$) [60]. The implication of this is that the compounds **L**₁-**L**₃ will not be soluble should they be considered as drugs because they will not be bioavailable in the systemic circulation if orally administered. The compounds showed reasonable binding energy with the targets (**Figure 9**). With the drug target 2J5F, phosphoryl-substituted urea **L**₂ showed comparable binding affinities with both the co-crystallized ligand and the standard drug doxorubicin (**Table 3**). The carboxylate and phosphonate ester groups significantly increased the binding affinities of the synthesized compounds (**L**₁ and **L**₂) when compared to **L**₃ without such groups (**Table 3**). There appears to be no significant difference in the binding affinities of carboxylate urea **L**₁ and the phosphonate urea **L**₂ against the two tested drug targets. The phosphoryl urea **L**₂ showed higher binding affinity with the drug target 2J5F, with the two scoring functions (London dG and 2J5F). Compound **L**₂ against 2J5F showed no significant difference in its binding affinity when compared to co-crystallized ligand but showed slight differences with the standard drug (doxorubicin).

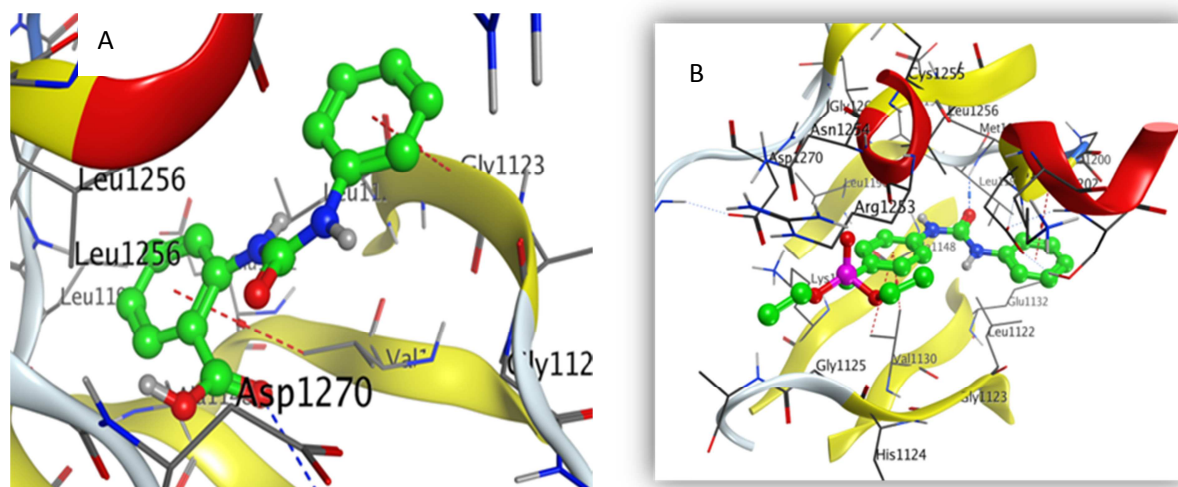


Figure 9: The binding mode of drug target 2J5F with (A) compound **L₁** (B) compound **L₂**. Note; blue dotted line = hydrogen bond; red dotted line = Pi bond

3.6.1. Chemical interaction of epidermal growth factor receptor kinase - EGFR kinase (2J5F) and anaplastic lymphoma kinase (5J7H) with target drug doxorubicin and urea ligands **L₁** and **L₂**

A number of amino acid residues from the epidermal growth factor receptor kinase – EGFR Kinase (2J5F) interacted with the standard drug doxorubicin, and a complex involving the following amino acids were formed; ASP 855, ARG 841, ASN 842, GLU 762, LEU 844, ALA 743, VAL 726, ASP 800, LEU 718, GLY 719, CYS 797 (**Figure S13**). The urea **L₁** interacted favourably with 8 amino acid residues including ASP 855, GLU 762, LEU 844, ALA 743, VAL 726, LEU 718, THR 854 and LYS 745 (**Figure S14**), while ASP 855, PHE 723, LEU 844, ALA 743, LEU 718, THR 854 and CYS 797 and LYS 745 were involved in complex formation with urea **L₂** (**Figure S15**). Similar binding interactions were observed for the anaplastic lymphoma kinase (5J7H) receptor where hydrogen bonding interactions were observed between ASP 1203 and ASP 1270 amino acid proteins of 5J7H and N12 and C30 of the doxorubicin with bond distances of 2.98 and 3.65Å respectively. There was also H-acceptor interaction between the O8 and LYS 1150 at a distance of 3.17Å. The study also showed ionic bonding interaction of N12 with ASP 1203 through its OD1 and OD2 at a distance of 3.32 and 2.98 Å respectively. 5LEU 1122 and GLY 1202 and 6-membered rings of doxorubicin interacted through pi-H bonding.

Essentially ASP 1203, ASP 1270, LYS 1150, LEU 1122 and GLY 1202 of anaplastic lymphoma kinase were responsible for doxorubicin binding to the receptor. In the urea **L**₁, the phenyl rings interacted with ASP 1203 through pi-H bonding at a distance of 4.44 Å. N1 and O1 of the urea bonded with MET 1199 at distances of 3.10 and 2.90 Å respectively. Other pi-H bonding interactions were observed between **L**₁ and **L**₂ with other amino acid residues LEU 1122, VAL 1130, GLY 1202 and ASP 1203.

4. Conclusion

Asymmetrically substituted ureas containing COOH and P=O hydrogen bond acceptor functional groups were synthesized and structurally characterized. The crystal structure of the carboxyl substituted urea **L**₁ indicated structural rearrangement of the predicted 1-D α -tape motif of the urea to a 2-D hydrogen bond chain of carboxylic acid dimer and a linear α -urea chain. The presence of the P=O in the urea **L**₂ resulted in the distortion of the predictable hydrogen bonding architecture of urea to a phosphoryl directing hydrogen-bonded tetramer. The carbonyl groups of the ureas were not involved in hydrogen bonding for the two compounds. NCI analysis revealed strong inter/intramolecular hydrogen bonding interactions in the urea compounds, indicating that the carboxyl and phosphoryl directing structures are probably the thermodynamically preferred structures in the crystal lattice. The protein and DNA docking results show increased binding affinities for the ureas containing carboxylate **L**₁ and phosphoryl **L**₂ functional groups relative to the urea without these functional groups **L**₃. Comparable ionic, hydrogen bonding and π -binding interactions were observed for the studied ureas and the standard drug doxorubicin.

Acknowledgment

The authors acknowledge Dr. Judith Burrows for the X-ray intensity data and Assoc Professor Graham Saunders for help with X-ray structure solution, University of Waikato, New Zealand, for funding and Tertiary Education Trust Fund Nigeria, for a scholarship to O.C.O.

Competing Interests.

We declare that none of the authors have any competing interests in the manuscript

Appendix A: Supplementary material

CCDC 1915786-1915787 contain the supplementary crystallographic data for compounds **L1** and **L2**. These data can be obtained free of charge via <http://www.ccdc.cam.ac.uk/conts/retrieving.html> (or from the Cambridge Crystallographic Data Centre, 12, Union Road, Cambridge CB2 1EZ, UK; fax: +44 1223 336033).

References

- [1] H. Fenniri, P. Mathivanan, K.L. Vidale, D.M. Sherman, K. Hallenga, K.V. Wood, J.G. Stowell, Helical rosette nanotubes: design, self-assembly, and characterization, *J. Am. Chem. Soc.* 123 (2001) 3854-3855.
- [2] P.A. Kollman, Hydrogen bonding and donor—acceptor interactions, in: H.F. Schaefer (Ed.), *Applications of Electronic Structure Theory*, Springer New York, NY, 1977, pp. 109-152.
- [3] E.R. Johnson, S. Keinan, P. Mori-Sanchez, J. Contreras-Garcia, A.J. Cohen, W. Yang, Revealing noncovalent interactions, *J. Am. Chem. Soc.* 132(18) (2010) 6498-6506.
- [4] G.R. Desiraju, Hydrogen bridges in crystal engineering: interactions without borders, *Acc. Chem. Res.* 35 (2002) 565-573.
- [5] J. Bernstein, M.C. Etter, L. Leiserowitz, The role of hydrogen bonding in molecular assemblies, *Struct. Correl.* 1 (2008) 431-507.
- [6] R. Custelcean, J.E. Jackson, Dihydrogen bonding: structures, energetics, and dynamics, *Chem. Rev.* 101 (2001) 1963-1980.
- [7] L.R. Sreenivas, S. Basavoju, V.R. Vangala, A. Nangia, Hydrogen Bonding in Crystal Structures of N, N'-Bis (3-pyridyl) urea. Why Is the NH---O Tape Synthons Absent in Diaryl Ureas with Electron-Withdrawing Groups?, *Cryst. Growth Des.* 6 (2006) 161-173.
- [8] R. Wechsel, M. Žabka, J.W. Ward, J. Clayden, Competing hydrogen-bond polarities in a dynamic oligoureia foldamer: A molecular spring torsion balance, *J. Am. Chem. Soc.* 140 (2018) 3528-3531.
- [9] S. Saha, G.R. Desiraju, A hand-twisted helical crystal based solely on hydrogen bonding, *Chem. Commun.* 53 (2017) 6371-6374.
- [10] S. Scheiner, 11 The Nature of the Hydrogen Bond, from a Theoretical Perspective, in: J.J. Novoa (Ed.), *Intermolecular Interactions in Crystals: Fundamentals of Crystal Engineering*, Royal Society of Chemistry, London, U.K., 2017, pp. 410-452.
- [11] J. Contreras-García, W. Yang, E.R. Johnson, Analysis of hydrogen-bond interaction potentials from the electron density: integration of noncovalent interaction regions, *J. Phys. Chem. A* 115 (2011) 12983-12990.
- [12] M.C. Gimeno, R.P. Herrera, Hydrogen Bonding Networks in Chiral Thiourea Organocatalysts: Evidence on the Importance of the Aminoindanol Moiety, *Cryst. Growth Des.* 16 (2016) 5091-5099.
- [13] K.H. Møller, A.S. Hansen, H.G. Kjaergaard, Gas Phase Detection of the NH—P Hydrogen Bond and Importance of Secondary Interactions, *J. Phys. Chem. A* 119 (2015) 10988-10998.
- [14] A. Mukherjee, S. Tothadi, G.R. Desiraju, Halogen bonds in crystal engineering: Like hydrogen bonds yet different, *Acc. Chem. Res.* 47 (2014) 2514-2524.
- [15] G.R. Desiraju, Reflections on the hydrogen bond in crystal engineering, *Cryst. Growth Des.* 11 (2011) 896-898.
- [16] N. Qureshi, D.S. Yufit, K.M. Steed, J.A.K. Howard, J.W. Steed, Anion hydrogen bonding from a 'revealed' urea ligand, *CrystEngComm* 18 (2016) 5333-5337.

- [17] A. Casula, M. Fornasier, R. Montis, A. Bettoschi, S.P. Argent, A.J. Blake, V. Lippolis, L. Marongiu, G. Picci, J.P. Tidey, Halogen-substituted ureas for anion binding: solid state and solution studies, *Supramol. Chem.* 29 (2017) 875-886.
- [18] P. Howlader, P. Das, E. Zangrando, P.S. Mukherjee, Urea-functionalized self-assembled molecular prism for heterogeneous catalysis in water, *J. Am. Chem. Soc.* 138 (2016) 1668-1676.
- [19] J. Świergiel, L. Bouteiller, J. Jadzyn, Hierarchical Structure of Supramolecular Polymers Formed by N, N'-Di (2-ethylhexyl) urea in Solutions, *J. Phys. Chem. B* 119 (2015) 12947-12953.
- [20] K. Yabuuchi, E. Marfo-Owusu, T. Kato, A new urea gelator: incorporation of intra-and intermolecular hydrogen bonding for stable 1D self-assembly, *Org. Biomol. Chem.* 1 (2003) 3464-3469.
- [21] H.M. Coubrough, C.D. Jones, D.S. Yufit, J.W. Steed, Gelation by histidine-derived ureas, *Supramol. Chem.* 30 (2018) 384-394.
- [22] R. Custelcean, Crystal engineering with urea and thiourea hydrogen-bonding groups, *Chem. Commun.* (2008) 295-307.
- [23] F. Lortie, S. Boileau, L. Bouteiller, N, N'-Disubstituted Ureas: Influence of Substituents on the Formation of Supramolecular Polymers, *Chem. Eur. J.* 9 (2003) 3008-3014.
- [24] R. Custelcean, B.A. Moyer, B.P. Hay, A coordinatively saturated sulfate encapsulated in a metal-organic framework functionalized with urea hydrogen-bonding groups, *Chem. Commun.* (48) (2005) 5971-5973.
- [25] J.T. Lenthall, J.A. Foster, K.M. Anderson, M.R. Probert, J.A.K. Howard, J.W. Steed, Hydrogen bonding interactions with the thiocarbonyl π -system, *CrystEngComm* 13 (2011) 3202-3212.
- [26] M. Asif, Short notes on diaryl ureas derivatives, *J. Adv. Res. Biochem. Pharmacol.* 1 (2018) 38-41.
- [27] G.O. Lloyd, J.W. Steed, Supramolecular assembly in a Janus-type urea system, *Chem. Commun.* 50 (2014) 1426-1428.
- [28] R. Custelcean, M.G. Gorbunova, P.V. Bonnesen, Steric Control over Hydrogen Bonding in Crystalline Organic Solids: A Structural Study of N, N'-Dialkylthioureas, *Chem. Eur. J.* 11 (2005) 1459-1466.
- [29] Rigaku Oxford Diffraction, CrysAlisPro Software System, version 1.171. 38.41 I, Rigaku Corporation, Oxford, UK, (2015).
- [30] O.V. Dolomanov, L.J. Bourhis, R.J. Gildea, J.A.K. Howard, H. Puschmann, OLEX2: a complete structure solution, refinement and analysis program, *J. Appl. Crystallogr.* 42 (2009) 339-341.
- [31] M. Frisch, G. Trucks, H. Schlegel, G. Scuseria, M. Robb, J. Cheeseman, G. Scalmani, V. Barone, B. Mennucci, G. Petersson, Gaussian, Inc., Wallingford CT (2009).
- [32] J. Valgeirsson, E.Ø. Nielsen, D. Peters, T. Varming, C. Mathiesen, A.S. Kristensen, U.I. Madsen, 2-Arylureidobenzoic acids: selective noncompetitive antagonists for the homomeric kainate receptor subtype GluR5, *J. Med. Chem.* 46 (2003) 5834-5843.
- [33] K. Tsutsumi, T. Sugimoto, Y. Tsuda, E. Uesaka, K. Shinomiya, Y. Shoji, A. Shima, Method for treating hyperlipidemia, Google Patents, 1992.
- [34] X. Zhao, Y.L. Chang, F.W. Fowler, J.W. Lauher, An approach to the design of molecular solids. The ureylene dicarboxylic acids, *J. Am. Chem. Soc.* 112 (1990) 6627-6634.
- [35] M.C. Etter, Z. Urbanczyk-Lipkowska, M. Zia-Ebrahimi, T.W. Panunto, Hydrogen bond-directed cocrystallization and molecular recognition properties of diarylureas, *J. Am. Chem. Soc.* 112(23) (1990) 8415-8426.
- [36] S.R. L, S. Basavoju, V.R. Vangala, A. Nangia, Hydrogen bonding in crystal structures of N, N'-bis (3-pyridyl) urea. Why is the N-HO tape synthon absent in diaryl ureas with electron-withdrawing groups?, *Cryst. Growth Des.* 6 (2006) 161-173.
- [37] M.C. Etter, Encoding and decoding hydrogen-bond patterns of organic compounds, *Acc. Chem. Res.* 23 (1990) 120-126.
- [38] R.F. Bader, A quantum theory of molecular structure and its applications, *Chem. Rev.* 91 (1991) 893-928.

- [39] J. Poater, M. Duran, M. Sola, B. Silvi, Theoretical evaluation of electron delocalization in aromatic molecules by means of atoms in molecules (AIM) and electron localization function (ELF) topological approaches, *Chem. Rev.* 105 (2005) 3911-3947.
- [40] S. Noury, X. Krokidis, F. Fuster, B. Silvi, Computational tools for the electron localization function topological analysis, *Comput. Chem. (Oxford)* 23 (1999) 597-604.
- [41] F. Zhou, R. Liu, P. Li, H. Zhang, On the properties of $S \cdots O$ and $S \cdots \pi$ noncovalent interactions: the analysis of geometry, interaction energy and electron density, *New J. Chem.* 39 (2015) 1611-1618.
- [42] B. Silvi, A. Savin, Classification of chemical bonds based on topological analysis of electron localization functions, *Nature* 371 (1994) 683-686.
- [43] R.F. Bader, T. Nguyen-Dang, Quantum theory of atoms in molecules—Dalton revisited, *Adv. Quantum Chem.* 14 (1981) 63-124.
- [44] E.R. Johnson, S. Keinan, P. Mori-Sanchez, J. Contreras-Garcia, A.J. Cohen, W. Yang, Revealing noncovalent interactions, *J. Am. Chem. Soc.* 132 (2010) 6498-6506.
- [45] A. Otero-de-la-Roza, E.R. Johnson, J. Contreras-García, Revealing non-covalent interactions in solids: NCI plots revisited, *Phys. Chem. Chem. Phys.* 14 (2012) 12165-12172.
- [46] C. Narth, Z. Maroun, R.A. Boto, R. Chaudret, M.-L. Bonnet, J.-P. Piquemal, J. Contreras-García, A complete NCI perspective: From new bonds to reactivity, in: R. Remi Chauvin, C. Christine Lepetit, B. Bernard Silvi, E. Alikhani (Eds.), *Applications of Topological Methods in Molecular Chemistry*, Springer, Switzerland, 2015, pp. 491-527.
- [47] R. Chaudret, B. De Courcy, J. Contreras-Garcia, E. Gloaguen, A. Zehnacker-Rentien, M. Mons, J.-P. Piquemal, Unraveling non-covalent interactions within flexible biomolecules: from electron density topology to gas phase spectroscopy, *Phys. Chem. Chem. Phys.* 16 (2014) 9876-9891.
- [48] J.N. Asegbeloyin, E.E. Oyeka, O.C. Okpareke, A. Ibezim, Synthesis, structure, computational and in-silico anticancer studies of N, N-diethyl-N'-palmitoylthiourea, *J. Mol. Struct.* 1153 (2018) 69-77.
- [49] J.N. Asegbeloyin, D.C. Izuogu, E.E. Oyeka, O.C. Okpareke, A. Ibezim, Crystal structure, non-covalent interaction and molecular docking studies of 2-[[2-phenylsulfonyl] hydrazinylidene] methyl} benzoic acid and its dysprosium catalysed cyclized product: 2-(phenyl-sulfonyl) phthalazin-1 (2H)-one, *J. Mol. Struct.* 1175 (2019) 219-229.
- [50] N.L. Henry, D.F. Hayes, Cancer biomarkers, *Mol. Oncol.* (2012) 140-146.
- [51] P. Seshacharyulu, M.P. Ponnusamy, D. Haridas, M. Jain, A.K. Ganti, S.K. Batra, Targeting the EGFR signaling pathway in cancer therapy, *Expert Opin. Ther. Targets* 16 (2012) 15-31.
- [52] J.R. Grandis, J.C. Sok, Signaling through the epidermal growth factor receptor during the development of malignancy, *Pharmacol. Ther.* 102 (2004) 37-46.
- [53] A. Wells, EGF receptor, *Int. J. Biochem. Cell Biol.* 31 (1999) 637-643.
- [54] R.D. Gascoyne, L. Lamant, J.I. Martin-Subero, V.S. Lestou, N.L. Harris, H.-K. Müller-Hermelink, J.F. Seymour, L.J. Campbell, D.E. Horsman, I. Auvigne, ALK-positive diffuse large B-cell lymphoma is associated with Clathrin-ALK rearrangements: report of 6 cases, *Blood* 102 (2003) 2568-2573.
- [55] C.A. Griffin, A.L. Hawkins, C. Dvorak, C. Henkle, T. Ellingham, E.J. Perlman, Recurrent involvement of 2p23 in inflammatory myofibroblastic tumors, *Cancer Res.* 59 (1999) 2776-2780.
- [56] Y.P. Mossé, M. Laudenslager, L. Longo, K.A. Cole, A. Wood, E.F. Attiyeh, M.J. Laquaglia, R. Sennett, J.E. Lynch, P. Perri, Identification of ALK as a major familial neuroblastoma predisposition gene, *Nature* 455 (2008) 930.
- [57] A.K. Murugan, M. Xing, Anaplastic thyroid cancers harbor novel oncogenic mutations of the ALK gene, *Cancer Res.* (2011) canres. 4041.2010.
- [58] H. Ren, Z.-P. Tan, X. Zhu, K. Crosby, H. Haack, J.-M. Ren, S. Beausoleil, A. Moritz, G. Innocenti, J. Rush, Identification of anaplastic lymphoma kinase as a potential therapeutic target in ovarian cancer, *Cancer Res.* 72 (2012).

[59] M. Soda, Y.L. Choi, M. Enomoto, S. Takada, Y. Yamashita, S. Ishikawa, S.-i. Fujiwara, H. Watanabe, K. Kurashina, H. Hatanaka, Identification of the transforming EML4–ALK fusion gene in non-small-cell lung cancer, *Nature* 448 (2007) 561.

[60] C.A. Lipinski, Lead-and drug-like compounds: the rule-of-five revolution, *Drug Discovery Today: Technologies* 1(4) (2004) 337-341.

Figure captions

Figure 1: One-dimensional α -tape urea chain.

Figure 2: Molecular structure of the *N,N'*-(2-carboxyl phenyl)phenyl urea **L**₁. Ellipsoids are drawn at 50% probability.

Figure 3: Interplay of inter and intra-molecular hydrogen bonding in the structure of **L**₁. The intramolecular bonds are shown in red while the intermolecular bonds are green in color. The relative proximity of the carboxyl oxygen to the urea NH contributes to the distortion of the usual α -tape synthon prevalent in di-substituted ureas.

Figure 4: Intermolecular CH----OH and NH----O=C stabilizing interactions in the hydrogen-bonded structure of **L**₁.

Figure 5: Molecular structure of **L**₂ showing two independent molecules in the asymmetric unit.

Figure 6: A side view of the hydrogen-bonded tetramer showing different hydrogen bond distances at each end of the tetramer.

Figure 7: (a) The plot of the reduced density gradient (s) against sign $\lambda(\rho)$ for the COOH dimer in the crystal structure of urea ligand **L**₁. (b) Gradient isosurface representation for carboxylic acid dimer ($s = 0.5$). The surfaces are scaled in blue, green and red coloration according to the sign $(\lambda_2)\rho$, from -0.2 to 0.2 a.u. Blue indicates strong, attractive interactions, and red indicates strong repulsive interactions or steric clashes.

Figure 8: The 2-D electron density plots for the phosphoryl urea dimer (top) and the corresponding 3-D isosurface representations (bottom) ($s = 0.5$ a.u.) ($-0.05 < \rho < 0.05$ a.u.).

Figure 9: The binding mode of drug target 2J5F with (A) compound **L**₁ (B) compound **L**₂. Note; blue dotted line = hydrogen bond; red dotted line = Pi bond

Journal Pre-proof

Two asymmetrically substituted ureas were synthesized and structurally characterized
Noncovalent interaction analysis revealed competitive hydrogen bonding interactions
Docking studies showed favorable binding between ureas and anticancer protein targets.

Journal Pre-proof